ISSN 1062-8738, Bulletin of the Russian Academy of Sciences: Physics, 2018, Vol. 82, No. 5, pp. 558–560. © Allerton Press, Inc., 2018.
Original Russian Text © A.V. Golenishchev-Kutuzov, V.A. Golenishchev-Kutuzov, R.I. Kalimullin, A.V. Semennikov, 2018, published in Izvestiya Rossiiskoi Akademii Nauk, Seriya Fizicheskaya, 2018, Vol. 82, No. 5.

Effect of Nanoscale Defects on the Physical Properties of Lithium Niobate and Lithium Tantalate Crystals

A. V. Golenishchev-Kutuzov[a], *, V. A. Golenishchev-Kutuzov[a], R. I. Kalimullin[a], and A. V. Semennikov[a]

[a]*Kazan State Power Engineering University, Kazan, 420066 Russia*

**e-mail: campoce6e@gmail.com*

Abstract—The elastic, ferroelectric, and transport properties of congruent lithium niobate and lithium tantalate crystals are studied in the temperature range of 77–450 K, depending on the conditions for recovery annealing. Significant changes in the elastic moduli and electrical conductivity that correlate with an increase in the displacement of the off-center Nb^{5+} (Ta^{5+}) ions along the trigonal $\bar{C}$ axis of the oxygen octahedra NbO_6 (TaO_6) are found in the interval 120 to 300 K as a result of more detailed studies. The attenuation of acoustic waves is suppressed as the temperature falls, which can be explained by an increase in the degree of ordering of NbO_6 (TaO_6) clusters. It may be assumed that the strong change in electrical conductivity correlates with the concentration of point nanoscopic defects (antisite defects Nb_{Li}^{5+} (Ta_{Li}^{5+}), coupled polarons Nb_{Li}^{4+} (Ta_{Li}^{4+}), and bipolarons).

DOI: 10.3103/S1062873818050118

INTRODUCTION

The wide use of lithium niobate (LN) and lithium tantalate (LT) crystals is based on their excellent physical properties characteristic of two states: either a stoichiometric composition (there are no impurity ions or micro- or nanodefects) or a congruent composition (containing impurity ions and micro- and nanodefects). The first type, LN and LT crystals of characterized by low values of their coercive fields ($E_C \le 10$ kV mm^{-1}) are used in the formation of periodic domain structures [1–3]. The second type of crystals has a wide variety of physical properties that depend on the nature of thermal annealing or the composition of impurity ions: electrical conductivity, unique photoinduced fields, and nonlinear optical and elastic characteristics. These features have allowed us to expand the use of LN and LT crystals in different laser and ultrasound devices [4–6].

A recent study of the formation of ferroelectric characteristics of LN and other transition metal oxides (ABO_3) in the region of high-temperature phase transitions ($T_{LN} \sim 1480$ K, $T_{LT} \sim 938$ K) [7, 8] of the order–disorder type, and the observed displacement of Jahn–Teller (JT) ions Nb^{5+} and Ta^{5+} to the off-center position in the octahedra of NbO_6 (TaO_6), provided a new view of the nature of photoinduced elastic and optical effects, and the transfer of electric charges. This applies in particular to congruent crystals whose physical properties change drastically when there are impurity JT ions (e.g., Fe^{2+}, Cr^{2+}, Cr^{4+}, or Cu^{2+}) or structural clusters formed by way of polarons or bipolarons (especially in the temperature range of 100–400 K, the one most important for practical applications). Many properties of congruent LN and LT crystals have yet to be fully explained (e.g., the structural anisotropy of electrical conductivity [9, 10] and polaron photoluminescence [11–14]).

EXPERIMENTAL

In [15], we performed a preliminary experimental study of the effect Nb^{5+} and Ta^{5+} JT ions in the temperature range of 500–80 K have on the elastic and ferroelectric properties of LN. However, the investigated samples were close in composition to stoichiometric ones (unannealed and without impurities). This prevented us from obtaining basic information on the role of Nb and Ta JT ions in the formation of elastic and electrical characteristics. Nevertheless, a smooth increase in the number of elastic moduli (C_{11} and C_{33}) and a decrease in acoustic attenuation α in the interval of 500–300 K were detected. This suggested the $Nb(Ta)O_6$ octahedra contract slightly along the trigonal $\bar{C}$ axis and expand along the $\bar{X}$ and $\bar{Y}$ axes as the temperature falls. These results confirmed the theoretical conclusions in [16] that there are aggregated point defect complexes at temperatures below 400 K. There was, however, no detailed study of such complexes.

Nominally pure samples of LN and LT (i.e., the concentration of iron, chromium and copper ions did

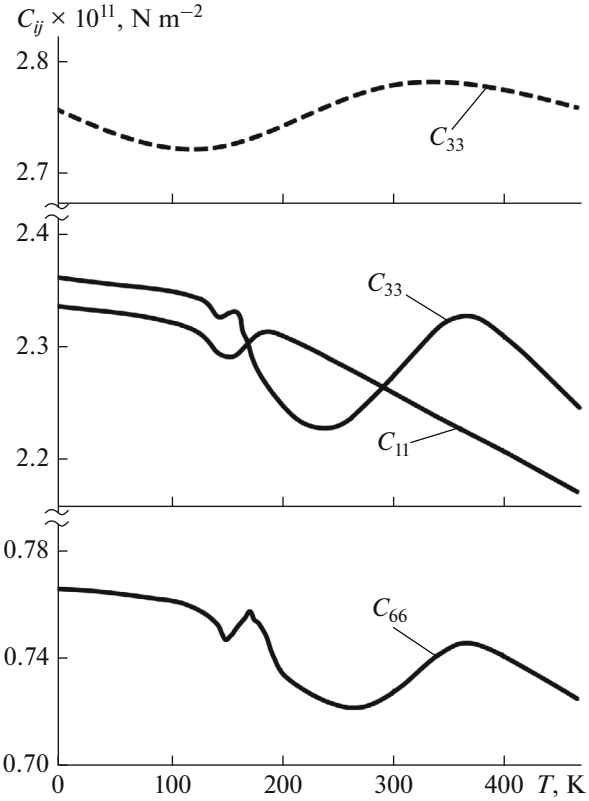

Fig. 1. Temperature dependences of elastic moduli: C_{11} (propagation of dilatational waves along the $\bar{X}$ and $\bar{Y}$ axes), C_{33} (propagation of dilatational waves along the $\bar{Z}$ axis), and C_{66} (propagation of transversal waves). Solid line is for $LiNbO_3$; dashed line is for $LiTaO_3$.

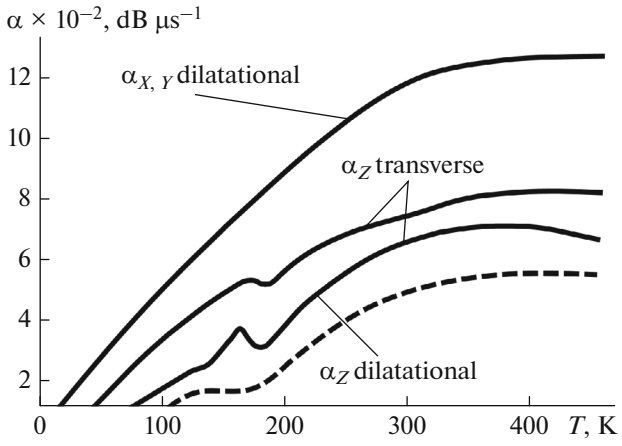

Fig. 2. Temperature dependences of acoustic attenuation α along axes $\bar{X}$, $\bar{Y}$ and $\bar{Z}$. The solid line is for $LiNbO_3$; the dashed line, for $LiTaO_3$.

not exceed 10^{15} cm^{-3}) were grown from a congruent melt at the Polyus Research Institute (Moscow) using the Czochralski technique. Eight such samples were used in a new stage of research performed on more sensitive equipment. All samples were subjected to recovery annealing in vacuum at different temperatures. Temperature variations (450–80 K) in the velocities and attenuation of acoustic waves at frequencies of 300–500 MHz were observed. We constructed the temperature dependences of elastic moduli C_{ij} and the attenuation of acoustic waves α for LN and LT (Figs. 1 and 2) using an earlier way of estimating the JT distortions of MnO_6 oxygen octahedra in lanthanum–strontium manganites [17], based on high-frequency ultrasonic measurements of elastic moduli.

Abrupt changes in the C_{11}, C_{33}, and C_{66} moduli in the temperature range of 120–340 K for the propagation of waves along axes $\bar{X}$ and $\bar{Z}$, and in their crystallographic anisotropy, were observed during the experiments. Changes in relative deformations ε_i of NbO_6 and TaO_6 octahedra, determined from the data for C_{ij} and α in the temperature range of 220–360 K, were averaged to produce the values presented in Table 1. There was an increase in ε_i in plane XY and a decrease in ε_i along the $\bar{Z}$ axis in both materials. Similar temperature changes in electrical conductivity, photoluminescence, and photoinduced fields were observed earlier for analogous congruent LN and LT crystals in the same temperature range [9, 10] (Fig. 3).

RESULTS AND DISCUSSION

Our new results can be explained by considering the properties of congruent materials and the conditions for recovery annealing. As is well known [1, 2, 4, 16], the ratio of Li/Nb ions is 0.95 in congruent LN, and some Nb^{5+} ions replace Li sites, forming defect Nb_{Li} centers (up to 1%). Nb^{5+} and Ta^{5+} are displaced along the trigonal axis with a change in the Nb–O and Ta–O distances in the NbO_6 and TaO_6 octahedra below the JT phase transition (T_C = 1483 K) from the paraelectric to the ferroelectric phase. The sharp changes in C_{ij} near 140–160 K are most likely related to the termination of ordering for the deformed NbO_6 or TaO_6 JT octahedra, which also can be seen from the temperature plots of electrical resistivity and photoluminescence (Fig. 3). This process is responsible for the

Table 1. Changes in relative deformations ε_i of NbO_6 and TaO_6 octahedra in the temperature range of 220–360 K

Samples	Deformation	
	ε_i (X, Y)	ε_i (Z)
$LiNbO_3$	2×10^{-4}	-1.3×10^{-3}
$LiTaO_3$	1.7×10^{-4}	-0.9×10^{-3}

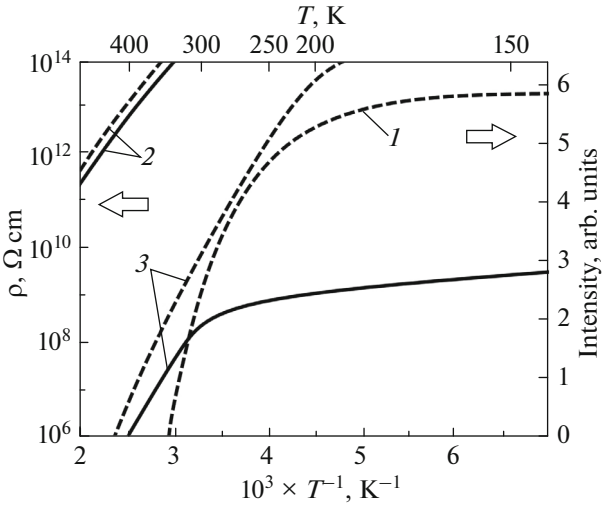

Fig. 3. Temperature dependences of (*1*) photoluminescence and specific electrical resistivity ρ for congruent $LiNbO_3$ samples (*2*) not annealed and (*3*) annealed in vacuum. Voltage was applied along axis $\bar{X}$ (solid line) or $\bar{Z}$ (dashed line). The laser beam propagated along axis $\bar{Z}$.

excellent ferroelectric characteristics of LN and LT, as follows from theoretical calculations [5–8].

The changes in elastic moduli observed in the range below 400 K can be attributed to the formation of different types of octahedra in this interval, with some of the Nb_{Nb} ions being replaced by Nb_{Li}, or Ta_{Ta} ions being replaced by Ta_{Li} (the latter are not JT ions). A change in the distance between Nb_{Nb} and the Nb–O ions in neighboring NbO_6 octahedra, or between Ta_{Ta} and the Ta–O ions in TaO_6 octahedra, can lead to rearrangement of the electron structure of LN (LT), and strong electron–phonon interaction can result in additional distortion of the NbO_6 or TaO_6 octahedra. The subsequent cooperative ordering along the trigonal axes of all octahedral, which ends in the temperature range below 120 K, can greatly alter the displacement nature of bipolarons and polarons of the Nb_{Li}^{4+}–Nb_{Nb}^{5+} and Nb_{Li}^{4+}–Nb_{Nb}^{4+} types, and thus the nature of the electrical conductivity and the photoinduced effects that were not explained earlier.

CONCLUSIONS

Our results show the effect JT ions have on the formation of ferroelectric and elastic characteristics, and on electrical conductivity and a number of photoinduced effects at temperatures below 400 K in congruent pure crystals of lithium niobate and lithium tantalate.

ACKNOWLEDGMENTS

This work was performed as part of State Task for Scientific Research no. 2014/448, project no. 2874.

REFERENCES

1. Volk, T. and Wohlecke, M., *Lithium Niobate: Defects, Photorefraction and Ferroelectric Switching*, Berlin: Springer, 2008.
2. *Ferroelectric Crystals for Photonic Applications*, Ferraro, P., Grilli, S., and De Natale, P., Eds., Berlin: Springer, 2009.
3. Shur, V.Y., in *Handbook of Advanced Dielectric, Piezoelectric and Ferroelectric Materials: Synthesis, Properties and Applications*, Ye, Z.-G., Ed., Cambridge: Woodhead, 2008, p. 622.
4. Malovichko, G., Grachev, V., and Schirmer, O., *Appl. Phys. B*, 1999, vol. 68, no. 5, p. 785.
5. Veithen, M. and Ghosez, Ph., *Phys. Rev. B*, 2002, vol. 65, no. 21, p. 214302.
6. Chaib, H., Otto, T., and Eng, L.M., *Phys. Rev. B*, 2003, vol. 67, no. 17, p. 174109.
7. Polinger, V., Garcia-Fernandez, P., and Bersuker, I.B., *Phys. B*, 2015, vol. 457, p. 296.
8. Toyoura, K., Ohta, M., Nakamura, A., and Matsunaga, K., *J. Appl. Phys.*, 2015, vol. 118, no. 6, p. 064103.
9. Akhmadullin, I.Sh., Golenishchev-Kutuzov, V.A., Migachev, S.A., and Mironov, S.P., *Phys. Solid State*, 1998, vol. 40, no. 7, p. 1190.
10. Yatsenko, A.V., Palatnikov, M.N., Sidorov, N.V., Pritulenko, A.S., and Evdokimov, S.V., *Phys. Solid State*, 2015, vol. 57, no. 8, p. 1547.
11. Harhira, A., Guilbert, L., Bourson, P., and Rinnert, H., *Appl. Phys. B*, 2008, vol. 92, no. 4, p. 555.
12. Garcia-Lechuga, M., Siegel, J., Hernandez-Rueda, J., and Solis, J., *J. Appl. Phys.*, 2014, vol. 116, no. 11, p. 113502.
13. Meyer, N., Nataf, G.F., and Granzow, T., *J. Appl. Phys.*, 2014, vol. 116, no. 24, p. 244102.
14. Golenishchev-Kutuzov, A.V., Golenishchev-Kutuzov, V.A., Kalimullin, R.I., and Semennikov, A.V., *Bull. Russ. Acad. Sci.: Phys.*, 2017, vol. 81, no. 3, p. 282.
15. Golenishchev-Kutuzov, A.V., Golenishchev-Kutuzov, V.A., Kalimullin, R.I., and Semennikov, A.V., *Phys. Solid State*, 2017, vol. 59, no. 2, p. 304.
16. Scrymgeour, D.A., Gopolan, V., Itagi, A., et al., *Phys. Rev. B*, 2005, vol. 71, no. 18, p. 184110.
17. Golenishchev-Kutuzov, A.V., Golenishchev-Kutuzov, V.A., Kalimullin, R.I., and Semennikov, A.V., *J. Low Temp. Phys.*, 2016, vol. 185, nos. 5–6, p. 558.

Translated by I. Obrezanova